Effect of overgrowth on shape, composition, and strain of SiGe islands on Si(001)

A. Hesse, J. Stangl, V. Holý,* T. Roch, and G. Bauer

Institut für Halbleiterphysik, Johannes Kepler Universität, A-4040 Linz, Austria

O.G. Schmidt and U. Denker

Max-Planck-Institut für Festkörperforschung, Heisenbergstrasse 1, D-70569 Stuttgart, Germany

B. Struth

European Synchrotron Radiation Facility, F-38043 Grenoble Cedex, France

We present a method and results based on x-ray scattering capable of resolving the shape and strain distribution in buried islands, as well as their vertical composition gradient. As an example, results are presented obtained for a single layer of SiGe dome-shaped islands capped by a 160-nm Si layer. For a growth temperature of 700 °C, a significant decrease of the average Ge content from about $x = 0.78$ before overgrowth to about $x = 0.37$ is found. The diameter of the islands increases from 110 to about 180 nm, their height shrinks from about 13 nm to 6 nm. This significant change of the island shape and content is accompanied by a pronounced change of their average in-plane lattice constant. The strain status of the overgrown flat islands is close to that of an embedded SiGe quantum well, i.e., with respect to the relaxation status of the uncapped islands a considerable strain redistribution takes place.

I. INTRODUCTION

Nowadays, an increasing effort is devoted to the fabrication and investigation of semiconductor nanostructures with controlled parameters. Apart from fundamental investigations of their structural, electronic, and optical properties, the exploitation of carrier confinement in quasi-zero-dimensional structures has already opened up the route to novel optoelectronical devices.[1,2] Nanostructures are also thoroughly investigated with respect to their potential for realizing solid-state-based quantum communication.[3]

The understanding of the formation processes of nanostructures is a prerequisite for their fabrication and application. Key parameters such as size, shape, chemical composition, and strain state of these nanostructures need to be controlled. In order to fabricate small three-dimensional islands with a high density, a growth instability, the Stranski-Krastanow growth mode, is widely used in the heteroepitaxy of semiconductors with a certain lattice mismatch. In this growth mode, three-dimensional islands emerge during the deposition of one semiconductor on top of another, because elastic strain relief in the islands lowers the total free energy of the heterosystem.[2] Depending on the materials involved, islands with sizes down to 12-nm base diameter and 2-nm height have been achieved.[4]

A series of studies exists on the size, shape, composition, and strain of such islands, involving many different analysis techniques. Direct imaging methods such as atomic force microscopy (AFM),[5–7] scanning tunneling microscopy (STM),[8] transmission electron microscopy (TEM)[9–12] are applied to obtain shape and size of islands. STM and TEM have also been used to investigate the chemical composition of islands. Techniques such as photoluminescence[13] and Raman spectroscopy[14,15] have led to an assessment of electronic properties and phonon confinement. Furthermore, several studies utilizing various x-ray scattering techniques have been published, which tackle the questions of size, shape, lateral correlations, as well as composition and strain distribution in such islands. For example, Schmidbauer *et al.* used grazing incidence small-angle x-ray scattering (GISAXS) to obtain information on the shape of uncapped SiGe pyramids on Si,[16] and with GISAXS also the shape and size of *buried* SiGe has been investigated.[17] The shape, composition, and strain of self-organized SiGe islands has been the topic of Refs. 18–22.

So far, x-ray studies of strain and composition in islands have been mainly restricted to the investigation of *uncapped* islands at a sample surface. Predominantly kinematical scattering theory has been used to simulate the scattered intensity. In many cases a fitting procedure with model assumptions is applied to obtain the strain and composition profiles in islands. A more direct method based on grazing incidence diffraction experiments has been presented in Refs. 23 and 24, but this method is restricted to uncapped islands as well.

However, for the investigation of their electronic and optical properties, uncapped islands cannot be used because of Fermi-level pinning at surface states. Thus for such purposes overgrowth of the islands is mandatory. Several investigations have shown that during overgrowth the shape, size, and strain status of these nanostructures may undergo substantial changes.[8,10,25–28] Consequently, the investigation of buried nanostructures is of utmost importance. So far, studies exist using TEM, employing advanced data analysis methods that yield in addition to shape and size also chemical information.[10,12,29] We show in this paper that for the investigation of buried islands, x-ray-diffraction experiments provide additional and also partly complementary information to that obtained from TEM. The main advantages of x-ray-diffraction (XRD) are the good statistical averaging, so that representative parameters for a large number of islands are

obtained, combined with a high sensitivity to the strain, and via strain also to the chemical composition. In such studies typically 10^6–10^8 islands contribute to the scattered signal.

We use high-resolution XRD to investigate the shape, strain, and composition in *buried* nanostructures. The approach is based on the measurement and simulation of reciprocal space maps, using model assumptions and a fitting process, as has already been applied to the case of uncapped islands.[21,22] In order to account for the decay of intensity for islands buried under a thick Si cap layer, the scattering process is described by distorted-wave Born approximation[30] instead of kinematical scattering theory only. Diffraction data and their analysis are presented for a sample with dome-shaped SiGe islands overgrown with a 160-nm-thick Si cap layer. The paper is organized as follows: in Sec. II the diffraction theory is presented, in Sec. III the sample parameters and the experimental XRD data are described. Section IV contains the analysis of results, which are discussed in Sec. V and summarized in Sec. VI.

II. THEORY

The scattering process for buried islands is described in the framework of the distorted wave Born approximation.[30,31] In this approach, we divide the scattering potential in the wave equation into two parts, the former describing the unperturbed system and the latter the perturbation. In the following, we deal only with the diffuse scattering and we will not consider the intensity distribution along the crystal truncation rod. Then, a semi-infinite "amorphous" substrate with constant polarizability χ_0 can be chosen as the unperturbed system, and both the crystalline structure of the surrounding matrix and the islands are included into the perturbation. Using this approach, the refraction of the primary and diffusely scattered beams at the sample surface are treated exactly; the waves propagating in the substrate are scattered kinematically from the crystal matrix and the islands. A more exact approach would consist in taking a semi-infinite crystalline substrate as the unperturbed system. In this case, the transmitted and diffracted waves in this system would be calculated dynamically and these waves would undergo a scattering process at the islands; only this process would be described kinematically. However, a numerical comparison of both approaches showed that significant differences in the diffusely scattered intensity appear only in points in reciprocal space, where the dynamical diffraction condition in the substrate is fulfilled for the incident and/or scattered beams, i.e., at the experimental monochromator and analyzer streaks and along the truncation rod. As the scattering signal from the buried islands and the surrounding strained Si matrix was found not to be affected by dynamical effects, we used the simpler approach with the "amorphous" unperturbed system.

The corresponding solutions for the wave equation are

$$|i\rangle = \begin{cases} \exp(-i\mathbf{K}_{i0}\cdot\mathbf{r}) + r_i\exp(-i\mathbf{K}_{iR}\cdot\mathbf{r}) & \text{for} \quad z>0 \\ t_i\exp(-i\mathbf{k}_{iT}\cdot\mathbf{r}) & \text{for} \quad z<0 \end{cases}$$

(1)

and

$$|f\rangle = \begin{cases} \exp(-i\mathbf{K}_{f0}\cdot\mathbf{r}) + r_f^*\exp(-i\mathbf{K}_{fR}\cdot\mathbf{r}) & \text{for} \quad z>0 \\ t_f^*\exp(-i\mathbf{k}_{fT}^*\cdot\mathbf{r}) & \text{for} \quad z<0. \end{cases}$$

(2)

Here we have denoted $\mathbf{K}_{i0}$ the wave vector of the incident wave in the solution $|i\rangle$, corresponding to the wave vector of the actual incident wave, see Fig. 1. The incident wave vector $\mathbf{K}_{f0}$ of the time-inverted solution $|f\rangle$ is the wave vector of the actual scattered wave. The wave vectors $\mathbf{K}_{i,fR}$ and $\mathbf{k}_{i,fT}$ denote the reflected and transmitted waves, respectively. $r_{i,f}$ and $t_{i,f}$ are the Fresnel reflection and transmission coefficients of both solutions. The z axis is parallel to the outward surface normal.

For capped islands, we only need to consider the part for $z<0$. In the investigated sample the positions of the islands are completely uncorrelated. The island density is still sufficiently low at about 6×10^8 cm^{-2} (see below), so that the decrease of the probability of finding an island in a close neighborhood of another island, which becomes important for very high island densities, plays no role for the intensity distribution in reciprocal space. Hence, in our case the diffusely scattered intensity is proportional to the intensity originating from a single dot

$$I = \text{const}\times|\langle f|\hat{\mathbf{V}}|i\rangle|^2,$$

(3)

where the perturbation of the scattering potential is given by

$$\hat{\mathbf{V}} = -K^2\Theta(-z)\{\chi_h(\mathbf{r})e^{i\mathbf{h}[\mathbf{r}-\mathbf{u}(\mathbf{r})]} - \chi_{hs}e^{i\mathbf{h}[\mathbf{r}-\mathbf{u}(\mathbf{r})]}\},$$

(4)

Where $\chi_h(\mathbf{r})$ is the local **h**th Fourier component of the polarizability of the sample depending on the island shape and its chemical composition, χ_{hs} is the polarizability component of the substrate, and $\Theta(-z)$ is the step function (unity for $z<0$ and zero for $z>0$). $\mathbf{u}(\mathbf{r})$ is the displacement field, which describes the deviations of the atom positions from the ideal lattice positions.

We introduce the coordinate system so that the diffraction vector has the coordinates

$$\mathbf{h} = h(\cos\xi,0,\sin\xi),$$

where ξ is the asymmetry angle of the diffraction, and we define the reduced scattering vector by

$$\mathbf{Q} = \mathbf{K}_{f0} - \mathbf{K}_{i0} - \mathbf{h} = (Q_x,0,Q_z),$$

i.e., we calculate the intensity distribution in the Q_xQ_z plane. The diffraction vector **h** lies in the same plane. Further, we assume that this reduced scattering vector is small compared to **h**. Then the matrix element can be written as

$$\langle f|\hat{\mathbf{V}}|i\rangle = -K^2t_it_f\int_{z<0}d^3\mathbf{r}\,e^{-i\mathbf{q}\mathbf{r}}\{\chi_h(\mathbf{r})e^{-i\mathbf{h}\mathbf{u}(\mathbf{r})} - \chi_{hs}\},$$

(5)

where we have denoted **q** the reduced scattering vector corrected to refraction and absorption. Due to the nearly rotationally symmetric shape of the dome-shaped islands found by AFM, we simplify the calculations assuming a cylindrical symmetry of $\mathbf{u}(\mathbf{r})$ and $\chi_h(\mathbf{r})$.
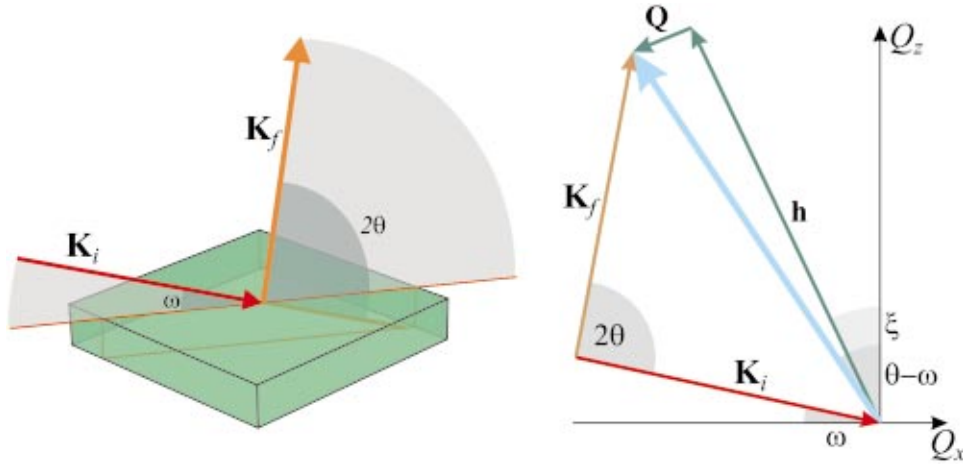
FIG. 1. (Color) Sketch of the coplanar scattering geometry in real space (left) and reciprocal space (right). Incident and scattered beams $\mathbf{K}_{i,f}$, and the surface normal lie in a common plane. The momentum transfer $\mathbf{h}$ with the asymmetry angle ξ and the reduced scattering vector $\mathbf{Q}$ are indicated as well.

For the calculation of the scattered intensity, we need to assume a model of the island shape and the profile of the chemical composition throughout the island. From this, the displacement field $\mathbf{u}(\mathbf{r})$ is obtained from field-emission microscopy (FEM) calculations using a three-dimensional model, taking the full elastic anisotropy into account. Then we use $\mathbf{u}(\mathbf{r})$ with $\mathbf{r}$ in the vertical plane containing the rotation axis and parallel to the reciprocal space map, and assume that this displacement field is cylindrically symmetric $\mathbf{u}(\rho,z)$ for the calculation of the diffraction pattern. We have proven by a series of numerical calculations that if we extract the displacement fields $\mathbf{u}(\mathbf{r})$ from the three-dimensional (3D) displacement distribution in different vertical planes, or use a full 3D simulation including the anisotropy, we do not get different results. However, it should be noted that this is due to the fact that the investigated sample is grown at a rather high temperature (see below), so that no pronounced facets of the buried islands are observed. For samples grown at

lower temperatures, it may become important to perform all calculations in 3D. Here, we may restrict the simulations to rotational symmetry, which allows us to speed up calculations by integrating the angular coordinate explicitly. This yields the expression for the simulation of the diffusely scattered intensity from the buried islands

$$\langle f|\hat{\mathbf{V}}|i\rangle = -2\pi K^2 t_i t_f \int_0^\infty d\rho\, \rho \int_{-\infty}^0 dz\, e^{-iq_z z}\{\chi_h(\rho,z)J_0(q_x\rho$$

$$+ h_x u_x(\rho,z))e^{-ih_z u_z(\rho,z)} - \chi_{hs}\}, \tag{6}$$

where J_0 is the Bessel function.

III. EXPERIMENT

A. Sample description

The investigated sample (S1213) was grown using solid source molecular-beam epitaxy on a Si (001) substrate. After
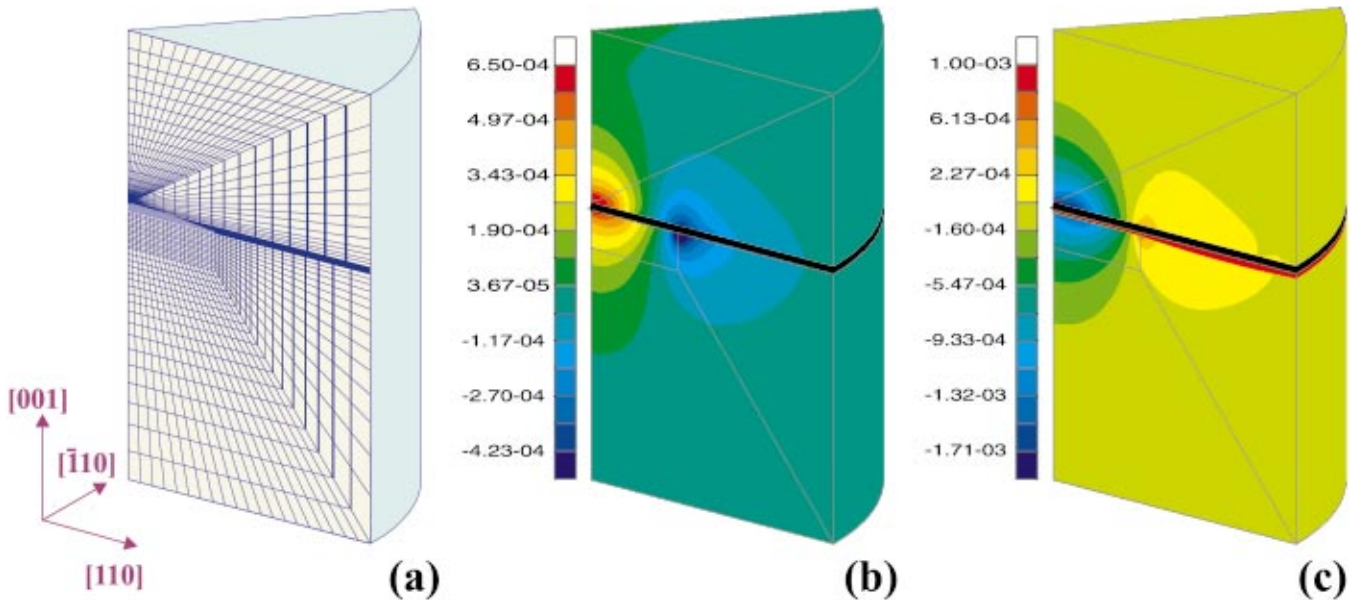

FIG. 2. (Color) (a) Finite element method (FEM) grid used for the simulations. The region of the island is indicated by the light gray area. The grid is first constructed in the (110) plane and extruded to a 45° wedge, taking advantage of the symmetry of the problem. (b) and (c) show the calculated in-plane and vertical strain components ε_{xx} and ε_{zz}.

a cleaning step at 900 °C, the substrate temperature was ramped down to the growth temperature of 700 °C while a Si buffer layer was grown. Then, 5 monolayers (ML) of Ge were deposited, followed by a 160-nm-thick Si cap layer, all grown at 700 °C. The Si growth rate was 0.1 nm/s. On top of the Si cap layer, another 5 ML of Ge have been deposited, forming a layer of uncapped islands, and their morphology was investigated by AFM. The height of the uncapped islands is 13 nm, their base diameter is about 110 nm, their density 6×10^8 cm^2. For the investigation of the buried islands with x-ray diffraction, this top layer has been etched off for 3.5 min using a mixture of 1 HF:2 H$_2$O$_2$:3 CH$_3$COOH. The sample investigated here has also been the scope of a previous investigation using TEM,[32] where the laterally averaged Ge profile along the [001] growth direction has been obtained from a numerical analysis of TEM data based on the digital analysis of lattice images (DALI).[29]

B. XRD measurements

X-ray-diffraction experiments were performed at the ESRF in Grenoble, France, at the TROÏKA II beamline (ID10B), using a wavelength of 1.55 Å. Reciprocal space maps (RSM's) have been recorded in a conventional coplanar diffraction setup, sketched in Fig. 1. Incident beam, scattered beam, and sample surface normal are within a common plane. In order to obtain information on the in-plane strain as well as on the strain along growth direction, we measured reciprocal maps around the asymmetrical (224) Bragg reflection of Si in two sample azimuths (incident beam along [110] and [1$\bar{1}$0]). The coplanar setup was chosen, because the investigation of buried islands requires a relatively large penetration depth of x-rays into the sample. Consequently, the use of grazing incidence reported previously for the study of uncapped islands[22] does not give any advantage. In XRD, the incident and exit angles $\alpha_{i,f}$ are well above the critical angle of total external reflection α_c, and a variation of $\alpha_{i,f}$ within the RSM plays no role. A measurement in the coplanar setup offers the advantage that a linear position sensitive detector can be used, decreasing significantly the measurement time per data point. As the scattered intensity from the buried islands is very weak, this allows to increase the integration time per point to several minutes in order to achieve sufficient counting statistics, while keeping the total time to record one map in the range of several hours.

Figure 3(a) shows the measured reciprocal (224) space map together with simulations. The Si substrate peak labeled "Si" is accompanied by a vertical truncation rod "TR," and diffuse scattering, presumably from point defects in the Si buffer and cap layers, visible around the substrate peak. The diffuse scattering from the islands and the deformation field around them gives rise to a broad maximum labeled "IL." This maximum is centered in reciprocal space at smaller q_z and q_x values with respect to the Si peak, thus it corresponds to both a larger in plane and larger vertical lattice parameters, corresponding to a partially relaxed SiGe island. [Here, we use the term relaxation with respect to the bulk lattice parameter of a SiGe alloy, i.e., $R = (a_\parallel - a_{Si})/(a_{SiGe} - a_{Si})$,
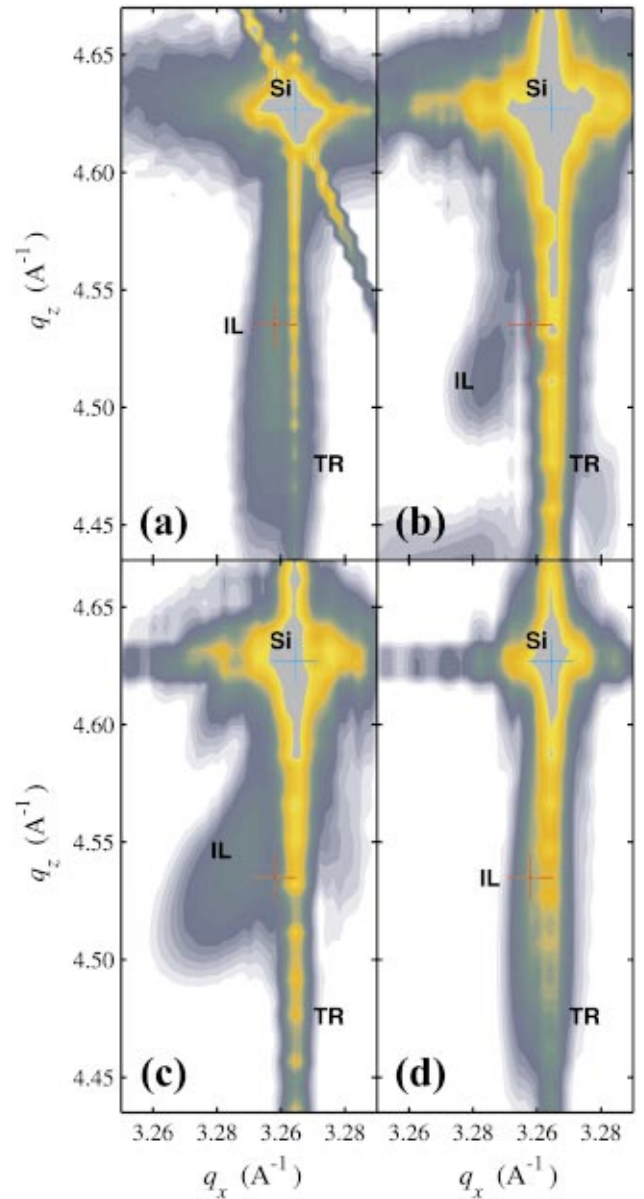

FIG. 3. (Color) Reciprocal space maps of the buried islands layer: (a) experiment; (b) simulation assuming the shape and Ge profile of uncapped islands from AFM and according to Ref. 22, respectively; (c) simulation for the same shape as (b), but optimized Ge profile; (d) simulation with both optimized Ge profile and optimized island shape. Contour levels are drawn in intervals of $10^{0.1}$. "Si" marks the (224) Si substrate peak, "TR" the coherent truncation rod, and "IL" is the intensity peak due to the partially relaxed SiGe islands. For easier comparison, blue marks indicate the substrate peak position and red marks indicate the experimental island peak position in all maps.

where $a_\parallel$ is the in-plane lattice paramter of the partially relaxed SiGe alloy, a_{SiGe} is its bulk lattice parameter, and a_{Si} is the bulk lattice parameter of Si.] From the FEM simulations described below, it is obvious that the lattice parameters of Si surrounding the island depend on the position. For instance, above and below the island the in-plane parameter is larger than a_{Si} and the vertical parameter is smaller. On the sides of the island, the in-plane parameter is smaller than a_{Si}. From
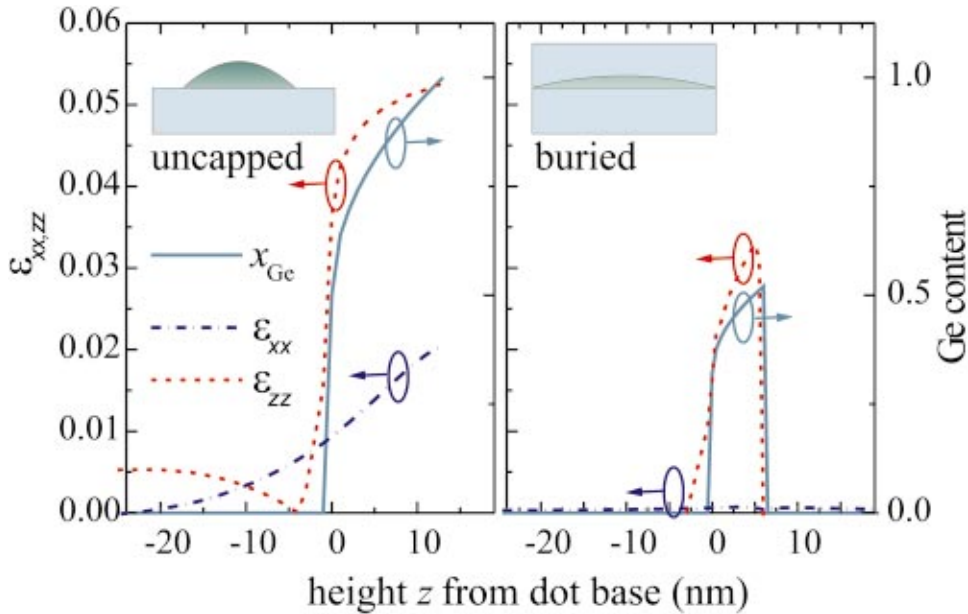
FIG. 4. (Color) Comparison of the in-plane strain along a vertical line through the center of the islands, and of the Ge profile for uncapped islands (a) (data taken from Ref. 22) and for the buried islands of this study (b). In the sketches, the height of the islands is exaggerated by a factor of 2.

this it follows that it is not possible to ascribe the observed maximum "IL" in Fig. 3 solely to the scattering process in the island volume.

The RSM measured around a 90° rotated azimuth revealed no difference, which indicates that the islands and their deformation field may be treated as rotationally symmetric, in accordance with the AFM image of the islands on the sample surface. This holds for our particular sample, which is grown at a high temperature. For samples grown at significantly lower temperatures around 500 °C, facetting has been observed even for capped islands.[8] For capping at a temperature of 700 °C, however, a significant shape change (accompanied by a change in the Ge content) is expected, smearing out the facets. Additionally, the already small elastic anisotropy of Si and SiGe is less important at higher temperatures.

IV. ANALYSIS OF THE XRD DATA

In order to analyze the structural properties of the buried islands, we use the fitting procedure described in Sec. II. Starting from an assumption on the shape, size, and the Ge profile of the buried islands, the strain distribution in and around a single "average" island is calculated using FEM. We model the island and the wetting layer as a sequence of layers. Figure 2(a) shows the FEM grid used for the calculation. The grid is first constructed in the (110) plane and extruded to a 45° wedge, taking advantage of the symmetry of the problem. The widths and the Ge content of these layers are chosen to reflect the shape and the Ge profile of the island (light gray area). Inside and in the close vicinity of the island, we use a mesh width of about 1 nm vertically and 3 nm horizontally. The FEM grid extends far into the substrate, and the density of the grid is gradually decreasing with distance from the island, where the elastic distortions are very small. The nodes at the bottom and at the circumference of the wedge are fixed. It has been checked that increasing the size of the simulation cell has no influence on the calculated displacement fields, i.e., the cell is "quasi-infinite." The

nodes at the side faces of the wedge can move only within the faces, but cannot move perpendicularly, according to the symmetry. The top surface of the grid is completely free and can relax elastically. We use a total number of about 40 000 nodes to calculate the displacement field in and around the islands, as well as the corresponding strain distribution, shown in Fig. 2(b,c). Using a slice through this three-dimensional strain distribution along the azimuth of the reciprocal space map, and assuming that the in-plane component is radially isotropic, the scattering signal is calculated numerically using Eq. (6) and compared to the measured intensity distribution. Then the shape, size, and Ge profile are refined until a reasonably good agreement between experiment and simulation is achieved. During this procedure it was tried to obtain a good agreement between the simulated and measured RSM's concerning the signal from the islands denoted "IL" in Fig 3. The diffuse scattering around the Si substrate and the truncation rod are not treated correctly by our simulations, as we do not include defect scattering. Furthermore, the width of the model lattice in the FEM calculations is smaller than the coherently illuminated area.

In order to keep the number of fitting parameters reasonably low, we approximate the shape of the islands by a truncated rotational paraboloid, where the height and the base and top radii are free parameters. In a series of simulations we found that the actual details of the shape, e.g., the presence of various facets, does not significantly influence the scattering pattern, but that the most important parameter is rather the aspect ratio $\eta = h/r_{base}$. This is especially true for buried islands, which are comparatively flat, and where the facets present for uncapped islands are "smeared out" due to interdiffusion and segregation of Ge during overgrowth at sufficiently high temperatures.

The Ge profile is assumed to vary only along growth direction, but not laterally. This is certainly not strictly true. However, as the profile obtained from the analysis is rather flat (see below), this model still describes the scattering from the islands reasonably well.

As starting point for the simulations of the scattered intensity, we used the height and lateral dimensions of the uncapped islands as measured by AFM for the top island layer, and assumed different Ge profiles, starting from a Ge content $x_{Ge,1}$ at the island base and increasing to $x_{Ge,2}$ at the island apex. For the variation of x_{Ge} along growth direction, we assumed a linear, quadratic, and square-root dependence (compare also Ref. 22). Figure 3(b) shows the calculated diffraction pattern for a square-root profile with $x_{Ge,1}=0.5$ and $x_{Ge,2}=1.0$, as was found for uncapped islands grown under the same conditions.[22] Obviously, neither position nor shape of the peak "IL" in the experimental data are reproduced correctly.

Varying $x_{Ge,1}$ and $x_{Ge,2}$, none of the profiles gives an acceptable correspondence with the experiment, as long as we do not alter the shape of the island. The "best fit" using the shape as obtained from AFM is shown in Fig. 3(c). In all simulations, the calculated position of the maximum intensity from the islands "IL" is at too small q_x. This indicates that actually the buried islands are less elastically relaxed than the simulated ones. Furthermore, the extension of the calculated intensity distribution along q_x and q_z does not match the measured one, indicating that the island shape is not correct. In order to obtain a less elastically relaxed island, generally two possibilities exist: (i) a reduction of the aspect ratio, as a flat island will relax less than a higher one; (ii) a reduction of the Ge content, because an island containing less Ge has a bulk lattice parameter closer to that of Si and consequently relaxes less than a Ge rich island. Of course, as the Ge content within the island is not constant, the terms "relaxation of the island" and "Ge content of the island" denote average quantities, and are used to indicate the trends.

Therefore, we made simulations for different island shapes, in particular, different aspect ratios η. As the measured peak "IL" is elongated along q_z, but narrow along q_x, it is obvious that the islands are rather flat. Using a diameter of the islands of 180 nm and a height of only 6 nm, we finally obtain a very good correspondence with the experimental data, see Fig. 3(d). Changing the height by 1 nm already yields a significant deviation from the experimental peak shape. Changing the island width has less effect on the result. As the islands are quite broad, from the experimental peak width a lower limit of the base diameter of 150 nm can be obtained. However, fluctuations of the Ge content of the islands as well as fluctuations of their aspect ratio increase the observed peak width, and the average diameter of the islands can be somewhat underestimated by our simulations.

As for the Ge content, the differences between the particular types of profiles, linear, square root, or quadratic, are very small, and choosing one or another type can be compensated by using slightly different parameters $x_{Ge,1,2}$. Depending on the particular profile we use, we obtain a Ge profile starting at $x_{Ge,1}=0.32\pm0.04$ at the island base, and reaching $x_{Ge,2}=0.52\pm0.04$ at its apex. The strain distribution corresponding to these parameters are shown in Fig. 2(b,c).

Compared to uncapped islands grown under the same conditions, for which we obtained $x_{Ge,1}=0.5$ and $x_{Ge,2}=1.0$,[22] a considerable *dilution* of the islands occurs
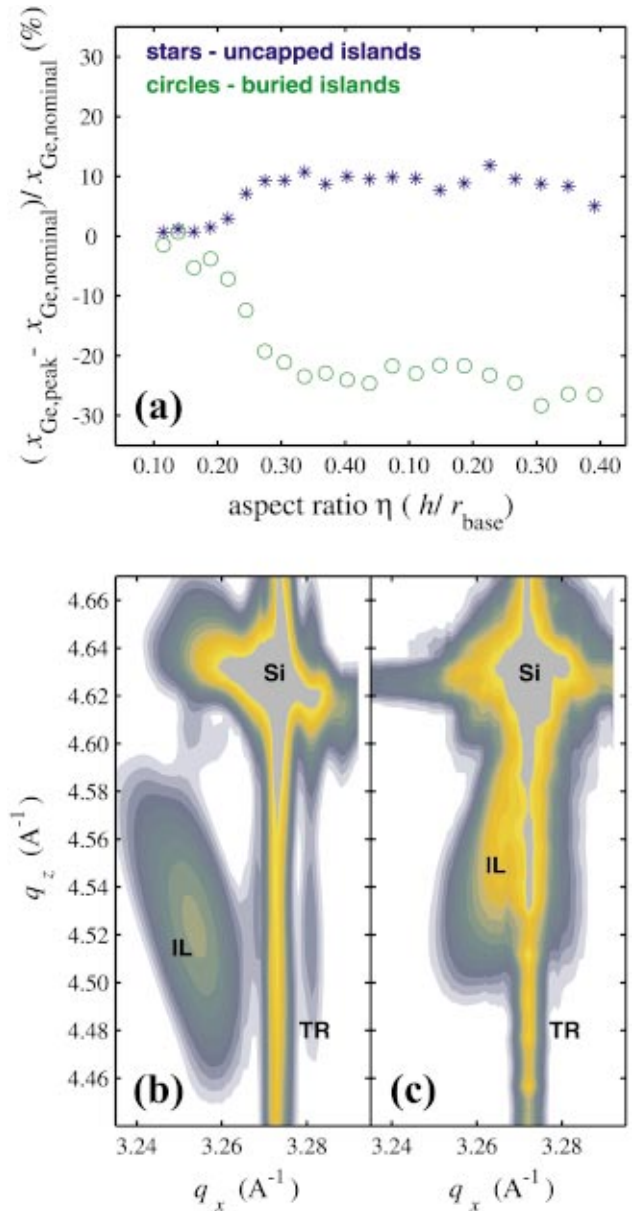

FIG. 5. (Color) (a) Deviation of Ge content of SiGe islands determined from a simple evaluation of peak positions from their actual content for various island aspect ratios in the case of uncapped (stars) and buried islands (circles). (b) Calculated intensity distribution for an uncapped SiGe island with an aspect ratio of $\eta=0.255$ and a Ge content of 37%. (c) Same as (b) for a buried island.

during overgrowth with Si. The aspect ratio is only $\eta=0.07$, much smaller than the value for uncapped islands $\eta=0.24$. Fluctuations of the island size lead to a change in the shape of the diffuse intensity distribution, whereas the maximum positions remains unaffected. The strain state of the buried islands is only slightly different from that of a two-dimensional layer. Figure 4 shows a comparison of the obtained values for shape, Ge content, and in-plane strain for uncapped islands at the sample surface [panel (a), taken from Ref. 22] and for the buried islands [panel (b)].

V. DISCUSSION

These results are also in good agreement with the shape and Ge profile determined previously using TEM and DALI. In fact, using the profile reported in Ref. 32 and the flat shape, we get a result matching the experiment equally well than the result described above. It has to be noted, however, that the DALI method yields unique results only in the case of very flat islands, where the slice of the specimen is thinner than the lateral extent of the buried islands. Otherwise, TEM averages over the island material and the surrounding Si "in front" and "behind" the island. Also in our x-ray analysis of buried islands, the scattered intensity stems not only from the islands themselves, but also from their deformed Si neighborhoods. This situation differs from the case of uncapped islands, where the main contribution to the scattered intensity originates from the islands. However, using a suitable model, the scattered intensity is described correctly independent of the island's aspect ratio, and the effect of the strained matrix surrounding the islands is included in the calculations.

The presence of this matrix has profound consequences for the analysis of the measured data. For uncapped islands, a rough numerical estimate on the content and strain can be obtained without elaborate simulations from the position of the maximum intensity in reciprocal space. For example, in Ref. 22 for uncapped SiGe domes on Si (001), from the simulations average values for in-plane strain and Ge content of 0.015 and 78% were obtained, while from the peak position values of 0.012 and 73% result. In order to demonstrate the problems encountered with buried islands, we performed a series of simulations for islands with different aspect ratios, and a constant composition of 37% Ge, corresponding to the average composition of the buried islands of this study. The displacement fields and the x-ray-diffraction patterns were calculated for both uncapped and buried islands *with the same shape*. From positions of the simulated intensity maxima we deduced the in-plane strain and the Ge content using simply Bragg's law and assuming a tetragonally distorted lattice in the islands. The deviation of the Ge content obtained from these peak positions from the actual one is plotted as a function of the aspect ratio in Fig. 5(a). Stars represent the results obtained for uncapped islands, circles those of the buried ones. Obviously, the simple analysis gives different results than a full simulation and fitting procedure. While the error remains below 12% (relative) for the uncapped islands, it increases with the aspect ratio up to 30% for the buried islands. This can be understood quite well qualitatively: an uncapped island is strained to the substrate only at its base, but otherwise free to relax elastically. Hence,

the assumption of tetragonal distortion of a SiGe alloy, which enters the determination of the average Ge content from the peak position alone, is approximately fulfilled. The same is true in the case of a buried, but very flat island, where the substrate exerts stress mainly from below and from the top, like for a 2D layer. Hence in these cases a quick analysis of peak positions, e.g., for the qualitative comparison of sample series, yields reasonable results. However, for buried islands with a high aspect ratio η, the surrounding matrix exerts stress in all directions, i.e., the hydrostatic stress component cannot be neglected any more. In this case, a more elaborate data analysis needs to be applied, and the peak positions can be used to follow trends only as long as the shape of the investigated islands is comparable.

This is immediately evident from Fig. 5(b,c), showing the intensity distribution for uncapped and buried islands with an aspect ratio of $\eta = 0.255$. Although the shape and content are the same in both cases, the maximum of scattered intensity appears at different positions in reciprocal space.

VI. CONCLUSIONS

In summary we have investigated the shape and composition profile of SiGe islands *buried* under a Si cap. A comparison to our previous study for uncapped islands yields a significant reduction in the Ge content of the islands, accompanied with a prominent change in the island shape. The Ge content varies between 32% at the island base and in the wetting layer to a maximum of 52% at the apex. The resulting average Ge content of 37% is significantly lower than for uncapped islands (78%), and the profile is much flatter for the buried islands. During overgrowth at a temperature of 700 °C, the islands flatten considerably. Their height decreases from about 13 nm to only 6 nm, while their base radius increases from 55 nm to 90 nm. Together with the decrease in the Ge content, this leads to a restraining of the island, as the average in-plane strain with respect to Si decreases from $\varepsilon_\parallel = 0.013$ to $\varepsilon_\parallel = 0.001$, i.e., the islands almost reach the strain state of a planar SiGe layer.

*Permanent address: Department of Solid State Physics, Faculty of Science, Masaryk University, 611 37 Brno, Czech Republic.

[1] P. Petroff, A. Lorke, and A. Imamoglu, Phys. Today **54**(5), 46 (2001).

[2] D. Bimberg, M. Grundmann, and N. N. Ledentsov, *Quantum Dot Heterostructures* (Wiley, Chichester, 1999).

[3] P. Michler, A. Kiraz, C. Becher, W.V. Schoenfeld, P.M. Petroff, L. Zhang, and A. Imamoglu, Science **290**, 2282 (2000).

[4] K. Eberl, O.G. Schmidt, S. Schieker, N.Y. Jin-Phillipp, and F. Phillipp, Solid-State Electron. **42**, 1593 (1998).

[5] S.A. Chaparro, Y. Zhang, J. Drucker, D. Chandrasekhar, and D.J. Smith, J. Appl. Phys. **87**, 2245 (2000).

[6] C.J. Huang, D.Z. Li, Z. Yu, B.W. Cheng, J.Z. Yu, and Q.M. Wang, Appl. Phys. Lett. **77**, 391 (2000).

[7] C.J. Huang, Y.H. Zuo, D.Z. Li, B.W. Cheng, L.P. Luo, J.Z. Yu, and Q.M. Wang, Appl. Phys. Lett. **78**, 3881 (2001).

[8] A. Rastelli, M. Kummer, and H. von Känel, Phys. Rev. Lett. **87**, 256101 (2001).

[9] M. Hammar, F.K. LeGoues, J. Tersoff, M.C. Reuter, and R.M. Tromp, Surf. Sci. **349**, 129 (1996).

[10] S.A. Chaparro, J. Drucker, Y. Zhang, D. Chandrasekhar, M.R. McCatney, and D.J. Smith, Phys. Rev. Lett. **83**, 1199 (1999).

[11] P.D. Miller, Chuan-Pu Liu, W.L. Henstrom, J. Murray Gibson, Y. Huang, P. Zhang, T.I. Kamins, D.P. Basile, and R. Stanley Williams, Appl. Phys. Lett. **75**, 46 (1999).

[12] Chuan-Pu Liu, J. Murray Gibson, D.G. Cahgill, T.I. Kamins, D.P. Basile, and R.S. Wiliams, Phys. Rev. Lett. **84**, 1958 (2000).

[13] O.G. Schmidt, and K. Eberl, Phys. Rev. B **61**, 13 721 (2000).

[14] K. Brunner, J. Zhu, G. Abstreiter, O. Kienzle, and F. Ernst, Thin Solid Films **369**, 39 (2000).

[15] M. Cazayous, J. Groenen, J.R. Huntzinger, A. Mlayah, and O.G. Schmidt, Phys. Rev. B **64**, 033306 (2001).

[16] M. Schmidbauer, Th. Wiebach, H. Raidt, M. Hanke, R. Köhler, and H. Wawra, Phys. Rev. B **58**, 10 523 (1998).

[17] J. Stangl, V. Holý, T. Roch, A. Daniel, G. Bauer, J. Zhu, K. Brunner, and G. Abstreiter, Phys. Rev. B **62**, 7229 (2000).

[18] M. Rauscher, R. Paniago, H. Metzger, Z. Kovats, J. Domke, J. Peisl, H.D. Pfannes, J. Schulze, and I. Eisele, J. Appl. Phys. **86**, 6763 (1999).

[19] Z. Kovats, M. Rauscher, H. Metzger, J. Peisl, R. Paniago, H.D. Pfannes, J. Schulze, I. Eisele, F. Boscherini, and S. Ferrer, Phys. Rev. B **62**, 8223 (2000).

[20] R. Paniago, H. Metzger, M. Rauscher, Z. Kovats, J. Peisl, J. Schulze, I. Eisele, and S. Ferrer, J. Appl. Crystallogr. **33**, 433 (2000).

[21] Th. Wiebach, M. Schmidbauer, M. Hanke, H. Raidt, R. Köhler, and H. Wawra, Phys. Rev. B **61**, 5571 (2000).

[22] J. Stangl, A. Daniel, V. Holy, T. Roch, G. Bauer, I. Kegel, T.H. Metzger, Th. Wiebach, O.G. Schmidt, and K. Eberl, Appl. Phys. Lett. **79**, 1474 (2001).

[23] I. Kegel, T.H. Metzger, A. Lorke, J. Peisl, J. Stangl, G. Bauer, J.M. García, and P.M. Petroff, Phys. Rev. Lett. **85**, 1694 (2000).

[24] I. Kegel, T.H. Metzger, A. Lorke, J. Peisl, J. Stangl, G. Bauer, and K. Nordlund, Phys. Rev. B **63**, 035318 (2001).

[25] P. Sutter, and M.G. Lagally, Phys. Rev. Lett. **81**, 3471 (1998).

[26] O.G. Schmidt, U. Denker, K. Eberl, O. Kienzle, and F. Ernst, Appl. Phys. Lett. **77**, 2509 (2000).

[27] F. Boscherini, G. Capellini, L. Di Gaspare, F. Rosei, N. Motta, and S. Mobilio, Appl. Phys. Lett. **76**, 682 (2000).

[28] G. Capellini, M. De Seta, and F. Evangelisti, Appl. Phys. Lett. **78**, 303 (2001).

[29] A. Rosenauer, U. Fischer, D. Gerthsen, and A. Förster, Appl. Phys. Lett. **71**, 3868 (1997).

[30] S.K. Sinha, E.B. Sirota, S. Garoff, and H.B. Stanley, Phys. Rev. B **38**, 2297 (1988).

[31] V. Holý, U. Pietsch, and T. Baumbach, *High Resolution X-Ray Scattering from Thin Films and Multilayers* (Springer, Berlin, 1999).

[32] U. Denker and O. G. Schmidt, Appl. Phys. Lett. (to be published).